International Year of CHEMISTRY 2011

Portugaliae Electrochimica Acta 2011, 29(5), 309-327

DOI: 10.4152/pea.201105309

PORTUGALIAE ELECTROCHIMICA ACTA
ISSN 1647-1571

Electron Reservoir Activity of High-Nuclearity Transition Metal Carbonyl Clusters

Fulvio Rossi and Piero Zanello*

Dipartimento di Chimica dell'Università di Siena, Via A. De Gasperi 2, 53100 Siena, Italy

Received 21 December 2010; accepted 3 Janeiro 2011

Abstract

Metal carbonyl clusters are molecules or molecular ions perfectly defined in size, composition and structural details, which belong by size to the field of nanomaterials. Their molecular structures result from subtle balances between the metal-metal and metal-carbonyl interactions and usually adopt close-packed structures in which a chunk of cubic or hexagonal metal lattice is surrounded by a shell of CO ligands.
Very often, such derivatives display extended redox activity affording reversible electron cascades. In many cases such activity increases if interstitial or semi-interstitial atoms of the main group elements (C, N, P, etc.) are inserted in their frames. This in fact triggers establishment of further metal-to-interstitial atom(s) interactions which not only contribute to the number of cluster valence electrons, but also modifies the bonding character of the frontier molecular orbitals.

Keywords: high-nuclearity metal-carbonyl clusters; molecular structures; electrochemistry.

Introduction

Miniaturization constitutes an actual and future challenge in developing mechanical, optical, and electronic devices. Metal clusters having a metallic core encapsulated in a ligand shell could be suitable candidates as components of data storage devices and could potentially represent the ultimate solution for miniaturization in nanoelectronics. [1]
As a matter of fact, metal–carbonyl clusters can be considered in principle as microscopic capacitors in that they are constituted by a kernel of metal atoms surrounded by a shell of nominally insulating carbonyl ligands, Fig. 1 [1a].

* Corresponding author. E-mail address: zanello@unisi.it
Plenary lecture at the XII Iberic Meeting of Electrochemistry and XVI Meeting of the Portuguese Electrochemical Society

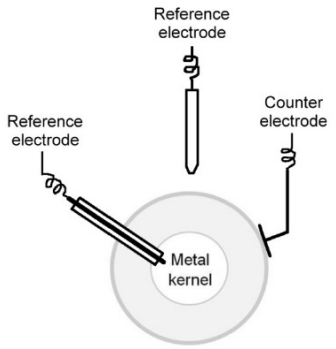

Figure 1. Schematic representation of a spherical capacitor constituted by a high-nuclearity metal carbonyl cluster.

Nevertheless, such a morphological similarity must be accompanied by a series of further requirements, such as:

1. electron-sink behavior, i.e. they should be able to accept and release electrons reversibly (or they must maintain unaltered their original molecular structure);
2. the carbonyl ligand shell should effectively insulate the metallic core in order to prevent intermolecular exchange of electrons, which would hinder effective storage of electrons in the core. In fact, easy intermolecular electron exchanges prevent the effective storage of electrons in the molecule. In this connection, evidences of the ability of metal cores of high-nuclearity metal carbonyl clusters to act as a quantum dot have been gained;
3. the metallic core of the cluster should possibly undergo transition from insulator-to-semiconductor regime;
4. finally, for practical purposes, the metallic core should display dimensions falling in the nanometric field.

The prerequisite to act as capacitor is to possess an extended and reversible redox behavior.

Interstitial or semi-interstitial atoms of the main group elements (C, N, P, etc.) play an essential role in the stabilization of high-nuclearity metal carbonyl clusters not only because they can contribute to the number of cluster valence electrons with no sterical consequences on the geometry of the cluster surface, but also because they can modify the bonding character of the frontier molecular orbitals.[2]

In this picture, we wish to give an overall survey of the redox propensity of a considerable number of metal-carbonyl clusters as it arises from electrochemical investigation.[3]

Homometallic clusters

Cobalt clusters

Let us start with the 130-CVE (Cluster Valence Electrons) dianion $[Co_9(\mu_8\text{-}P)(CO)_{21}]^{2-}$. Fig. 2 shows its monocapped square antiprismatic geometry

(encapsulating the phosphide atom) as well as its redox activity in MeCN solution. [4]

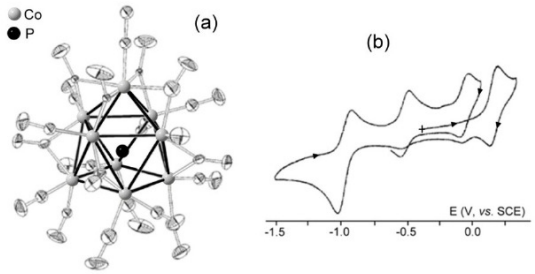

Figure 2. (a) Crystal structure and (b) cyclic voltammetric behavior (recorded at a platinum electrode in MeCN solution; scan rate 0.2 Vs^{-1}) of $[Co_9P(CO)_{21}]^{2-}$.

It exhibits a one-electron oxidation and a two-electron reduction, both of which are partially chemically reversible. In addition, both the redox processes are coupled to chemical complications which afford two new peak systems at intermediate potential values, which have been tentatively assigned to degradation of the electrogenerated species to the phosphide monoanion $[Co_6P(CO)_{16}]^{-}$.

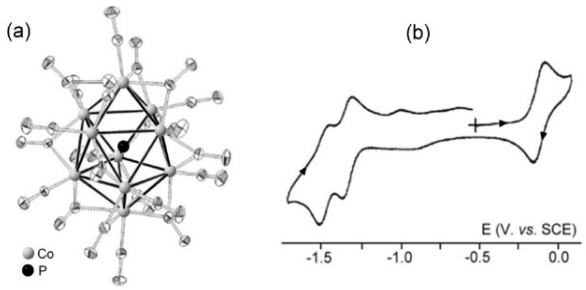

Figure 3. (a) Crystal structure and (b) cyclic voltammetric behavior (recorded at a platinum electrode in MeCN solution; scan rate 0.2 Vs^{-1}) of $[Co_{10}P(CO)_{22}]^{3-}$.

Related to the previous dianion is the 142-CVE bicapped square antiprismatic phosphide trianion $[Co_{10}(\mu_8\text{-}P)(CO)_{21}]^{3-}$, whose molecular structure and electrochemical behavior are illustrated in Fig. 3 [4]. As seen, it exhibits a redox pattern somewhat reminiscent that of $[Co_9P(CO)_{21}]^{2-}$, in that it undergoes a one-electron oxidation and two sufficiently separated one-electron reduction processes. All the processes exhibit partial chemical reversibility.

The formal electrode potentials of the redox changes exhibited by the two phosphide clusters are compiled in Table 1, together with those of related species that will be discussed below.

In confirmation that cobalt clusters with interstitial or semi-interstitial nitrogen atoms show a distinctive aptitude towards unusual stereochemistry and high coordination numbers, (i.e. affording quite spectacular shapes and extended electron transfer properties), let us consider the anions $[Co_{10}N_2(CO)_{19}]^{4-}$ and $[Co_{11}N_2(CO)_{21}]^{3-}$.

Fig. 4 shows the crystal structure [5a] and the cyclic voltammetric behavior in CH_3CN solution [5b] of the 142-CVE tetraanion $[Co_{10}N_2(CO)_{19}]^{4-}$.

Table 1. Formal electrode potentials [V, *vs*. SCE] for the electron transfer processes exhibited by the cobalt clusters under discussion. CH_3CN solution.

Complex	Oxidation processes			Reduction processes			
	$E°'_{4-/3-}$	$E°'_{3-/2-}$	$E°'_{2-/-}$	$E°'_{2-/3-}$	$E°'_{3-/4-}$	$E°'_{4-/5-}$	$E°'_{5-/6-}$
$[Co_9(\eta^8\text{-}P)(CO)_{21}]^{2-}$	-	-	+0.16	−1.00	−1.00	-	-
$[Co_{10}(\eta^8\text{-}P)(CO)_{22}]^{3-}$	-	−0.10	-	-	−1.32	−1.47	
$[Co_{10}N_2(CO)_{19}]^{4-}$	−0.85	−0.52	−0.14	-	-	−1.72	−2.16
$[Co_{11}N_2(CO)_{24}]^{3-}$	-	−0.23	−0.23	-	−1.05	−1.47	−2.07
$[Co_{13}C_2(CO)_{24}]^{4-}$	−0.54	-	-	-	-	−1.06	−1.68

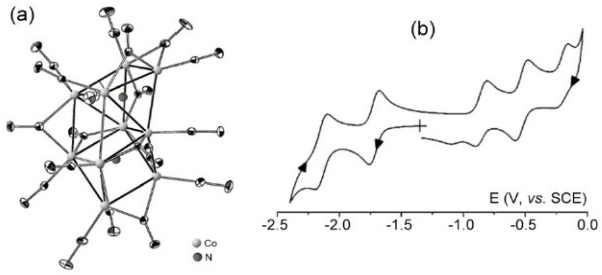

Figure 4. (a) Crystal structure and (b) cyclic voltammogram (recorded at a platinum electrode in MeCN solution; scan rate 0.2 Vs^{-1}) of $[Co_{10}N_2(CO)_{19}]^{4-}$.

The tetraanion (whose molecular structure can be seen as built from two trigonal prismatic units each containing an interstitial nitrogen atom, sharing a common edge) undergoes either three successive oxidations or two successive reductions, which, but for the most anodic step, exhibit features of chemical reversibility in the cyclic voltammetric time scale.

In confirmation of the complete chemical reversibility of such processes, cyclic voltammetric tests carried out on the solutions resulting from each exhaustive one-electron removal afforded profiles quite complementary to the original ones. Given the similar peak heights of the reduction processes, it follows that the present cluster can shuttle reversibly the rich sequence $[Co_{10}N_2(CO)_{19}]^{2-/3-/4-/5-/6-}$.

In turn, Fig. 5 shows the molecular structure and the voltammetric profile in CH_3CN solution of the 154-CVE trianion $[Co_{11}N_2(CO)_{21}]^{3-}$ [5b].

The trianion (whose molecular structure can be seen as two octahedrons having a common vertex, each octahedron encapsulating a nitrogen atom) exhibits three consecutive reductions and one oxidation process, each step involving one electron *per* molecule. The pertinent formal electrode potentials are summarized in Table 1.

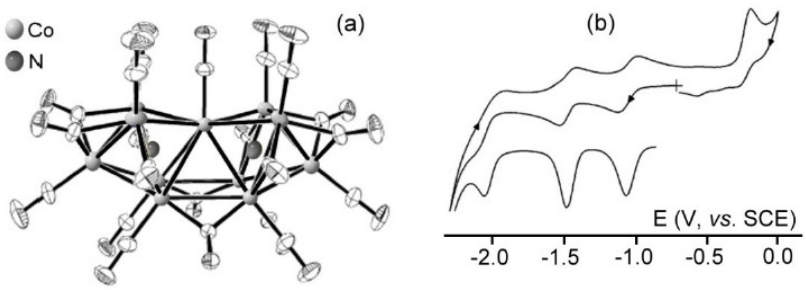

Figure 5. (a) Crystal structure of $[Co_{11}N_2(CO)_{21}]^{3-}$. (b) Cyclic and Osteryoung square wave voltammograms recorded at a platinum electrode in MeCN solution. Scan rates 0.2 Vs^{-1} and 0.1 Vs^{-1}, respectively.

The last example of the present section we discuss is the 177-CVE tridecacobaltate dicarbide tetranion $[Co_{13}C_2(CO)_{24}]^{4-}$. Its crystal structure can be described as two mutually rotated prismatic Co_6C units sharing a common vertex, capped at opposite sides by two five-bridging cobalt atoms, Fig. 6 [6a].

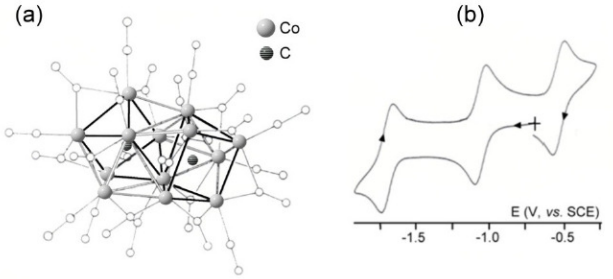

Figure 6. (a) Crystal structure of $[Co_{13}C_2(CO)_{24}]^{4-}$. (b) Cyclic voltammograms of $[Co_{13}C_2(CO)_{24}]^{4-}$ in CH_3CN solution. Platinum working electrode. Scan rate 0.2 Vs^{-1}.

As illustrated in Fig. 6b, the tetraanion exhibits one oxidation and two reduction processes, all having features of chemical and electrochemical reversibility. Each passage involves one electron [6b]. The formal electrode potentials of such redox changes are reported in Table 1.
We note that the related 176-CVE dinitride trianion $[Co_{13}N_2(CO)_{24}]^{3-}$ possesses a more limited redox activity [6b].

Iridium clusters

Two examples of iridium carbonyl cluster with quite spectacular molecular structures are here reported. The first example is constituted by the 158-CVE dianion $[Ir_{12}(CO)_{24}]^{2-}$, whose metallic frame can be simply described as a large (ν_2) *incomplete* trigonal bipyramid, in that it lacks one axial and one equatorial vertex, Fig. 7a [7]. In MeCN solution it undergoes a series of oxidations and reductions coupled to chemical complications. The most significant are the first two-electron oxidations and the first two-electron reductions illustrated in Fig. 7b [7].

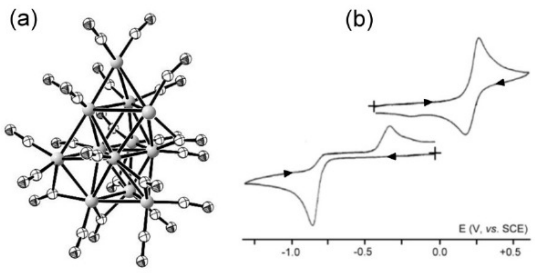

Figure 7. (a) X-Ray structure of $[Ir_{12}(CO)_{24}]^{2-}$. (b) Cyclic voltammograms recorded at a platinum electrode in CH_3CN solution. Scan rate 0.2 Vs^{-1}.

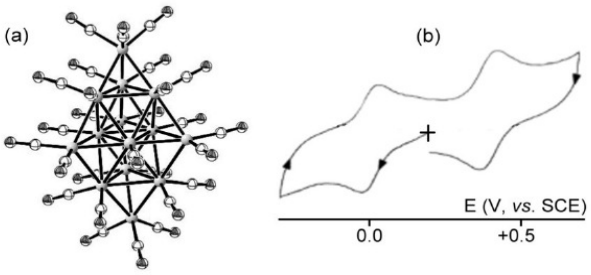

Figure 8. (a) X-Ray structure of $[Ir_{14}(CO)_{27}]^{-}$. (b) Cyclic voltammogram recorded at a platinum electrode in CH_3CN solution. Scan rate 0.2 Vs^{-1}.

In spite of features of chemical reversibility of the $[Ir_{12}(CO)_{24}]^{2-}/[Ir_{12}(CO)_{24}]^{0}$ oxidation, the electrogenerated neutral derivative suffers slow decomposition. As far as the $[Ir_{12}(CO)_{24}]^{2-}/[Ir_{12}(CO)_{24}]^{4-}$ reduction is concerned, although largely departing from the electrochemical reversibility (the high peak-to-peak separation attests its electrochemical quasireversibility), it resulted chemically reversible upon exhaustive electrolysis, thus supporting that the tetraanion undergoes a significant geometrical reorganization.

The second example is offered by the 181-CVE monoanion $[Ir_{14}(CO)_{27}]^{-}$, which is related to the preceding Ir_{12} dianion, in that it possesses the *complete* (ν_2) trigonal-bipyramidal geometry [8].

As illustrated in Fig. 8, the closed molecular arrangement of the Ir_{14} monoanion is sufficiently flexible to sustain reversibly either the $[Ir_{14}(CO)_{27}]^{-}/ [Ir_{14}(CO)_{27}]^{0}$ oxidation or the $[Ir_{14}(CO)_{27}]^{-}/ [Ir_{14}(CO)_{27}]^{2-}$ reduction [8].

The formal electrode potentials of the electron transfer processes exhibited by the Ir_{12} and Ir_{14} clusters are reported in Table 2.

Table 2. Formal electrode potentials [V, *vs*. SCE] for the electron transfer processes exhibited by the iridium clusters under discussion.

Complex	Oxidation processes				Reduction processes					solvent
	$E°'_{2-/-}$	$E°'_{-/0}$	$E°'_{0/+}$	$E°'_{+/2+}$	$E°'_{-/2-}$	$E°'_{2-/3-}$	$E°'_{3-/4-}$	$E°'_{4-/5-}$	$E°'_{5-/6-}$	
$[Ir_{12}(CO)_{24}]^{2-}$	+0.26[a]	+0.26[a]	+0.83[b]	+0.83[b]	-	−0.58[c]	−0.58[c]	−1.50[b]	−1.50[b]	MeCN
$[Ir_{14}(CO)_{27}]^{-}$	-	+0.39	-	-	0.00	-	-	-	-	CH_2Cl_2

[a] Coupled to slow chemical complications; [b] peak potential value for irreversible processes;
[c] electrochemically quasireversible.

Platinum clusters

The high-nuclearity platinum clusters $[Pt_{19}(CO)_{22}]^{4-}$, $[Pt_{24}(CO)_{30}]^{2-}$ and $[Pt_{38}(CO)_{44}]^{2-}$ exhibit an unexpected high aptitude to undergo reversible redox processes.

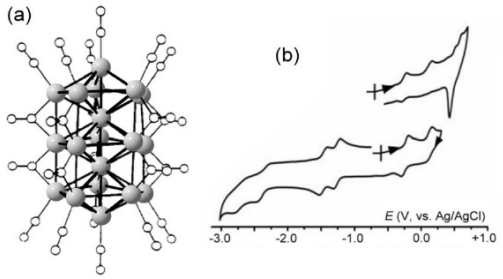

Figure 9. (a) X-Ray structure of $[Pt_{19}(CO)_{22}]^{4-}$. (b) Cyclic voltammograms recorded at a glassy carbon electrode in DMF solution. Scan rate 0.2 Vs^{-1}.

Let us start with the 230-CVE tetraanion $[Pt_{19}(CO)_{22}]^{4-}$. Its molecular structure consists of a stacked sequence of three pentagonal layers of platinum atoms, sandwiching two platinum atoms, and capped at opposite sides by one platinum atom, Fig. 9a [9]. As shown in Fig. 9b, it undergoes a sequence of close-spaced pairs of reversible one-electron processes, stepwise ranging from 0 to 8– overall charge [10].

It is noted that the electrogenerated neutral species $[Pt_{19}(CO)_{22}]^{0}$ undergoes adsorption to the electrode surface.

The pertinent redox potentials of the redox changes exhibited by the cluster are reported in Table 3, together with those of the mentioned platinum clusters discussed below.

Table 3. Formal electrode potentials [V, *vs*. Ag/AgCl] for the electron transfer processes exhibited by the platinum clusters under discussion.

Complex	Redox processes								Solvent
	$E°'_{0/-}$	$E°'_{-/2-}$	$E°'_{2-/3-}$	$E°'_{3-/4-}$	$E°'_{4-/5-}$	$E°'_{5-/6-}$	$E°'_{6-/7-}$	$E°'_{7-/8-}$	
$[Pt_{19}(CO)_{22}]^{4-}$	+0.62[a]	+0.53 [a]	+0.18[a]	–0.24	–1.25	–1.45	–2.38	–2.70	DMF
$[Pt_{24}(CO)_{30}]^{2-}$	+0.64[a]	+0.34	–0.47	–0.72	–1.22	–1.48	-	-	CH_2Cl_2
$[Pt_{38}(CO)_{44}]^{2-}$	+0.57[a]	+0.38	–0.32	–0.54	–0.93	–1.20	-	-	CH_2Cl_2

[a] Peak-potential values for irreversible processes (or for adsorbed species; see text).

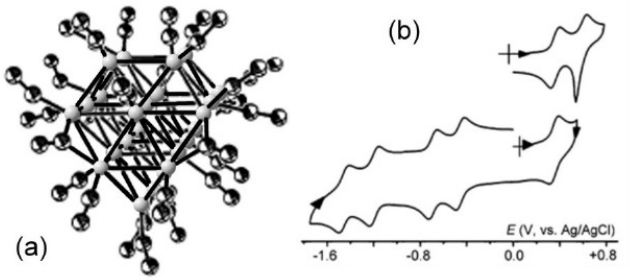

Figure 10. (a) X-Ray structure of $[Pt_{24}(CO)_{30}]^{2-}$. (b) Cyclic voltammograms recorded at a glassy carbon electrode in CH_2Cl_2 solution. Scan rate 0.2 Vs^{-1}.

As far as the 302-CVE dianion $[Pt_{24}(CO)_{30}]^{2-}$ is concerned, Fig. 10a shows its crystal structure, which has a cubic closest packing of Pt atoms constituted by four parallel planes of Pt atoms (4, 9, 8, 3); the nine platinum atoms layer contains an interstitial Pt atom.[11] The pertinent cyclic voltammetric profile shown in Fig. 10b indicates that it also undergoes reversibly a sequence of one-electron process, namely two oxidations and four reductions, according to the stepwise passage of the overall charge from 0 to 6–; see Table 3 [10, 11].
Also in this case, the electrogenerated neutral species $[Pt_{24}(CO)_{30}]^{0}$ is adsorbed at the electrode surface.
Finally, we discuss about the 470-CVE dianion $[Pt_{38}(CO)_{44}]^{2-}$, whose molecular structure, which is illustrated in Fig. 11a, consists of an overall ν_3 truncated octahedron [12]. As shown in Fig. 11b, its redox profile is reminiscent that of $[Pt_{24}(CO)_{30}]^{2-}$, in that it also undergoes reversibly the progressive passage of the overall charge from 0 to 6–; see Table 3 [10, 11].

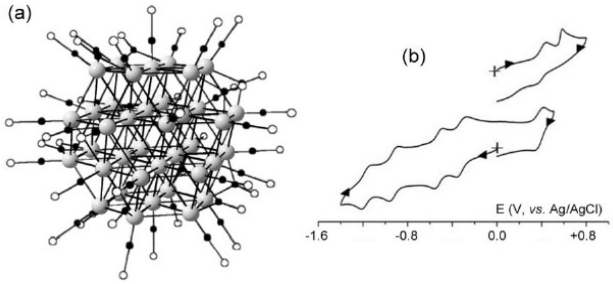

Figure 11. (a) X-Ray structure of $[Pt_{38}(CO)_{44}]^{2-}$. (b) Cyclic voltammograms recorded at a glassy carbon electrode in CH_2Cl_2 solution. Scan rate 0.2 Vs^{-1}.

Osmium clusters

We like to discuss shortly about the dianion $[Os_{20}(CO)_{40}]^{2-}$, the macro-tetrahedral geometry of which is shown in Fig. 12a [13]. Unpublished cyclic voltammetric data revealed a rich electrochemistry, which, based on the previously described behavior of platinum clusters, have been now tentatively reinterpreted according to the profile illustrated in Fig. 12b.

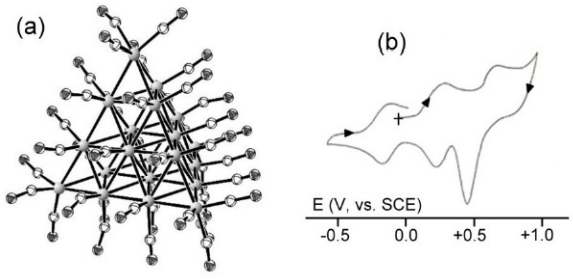

Figure 12. (a) Molecular structure of $[Os_{20}(CO)_{44}]^{2-}$. (b) Cyclic voltammogram recorded at a glassy carbon electrode in CH_2Cl_2 solution. Scan rate 0.2 Vs^{-1}.

It undergoes reversibly the oxidations $[Os_{20}(CO)_{44}]^{2-}/[Os_{20}(CO)_{44}]^{-}$ ($E°' = +0.32$ V) and $[Os_{20}(CO)_{44}]^{-}/[Os_{20}(CO)_{44}]^{0}$ ($E_p = +0.74$ V, accompanied by electrode

adsorption of the neutral species) and the reduction $[Os_{20}(CO)_{44}]^{2-}/[Os_{20}(CO)_{44}]^{3-}$ ($E^{\circ\prime} = -0.15$ V).

Nickel clusters

Concerned with extended the electrochemical activity of high-nuclearity Ni-cluster, two Ni-carbide deserve attention: $[Ni_{32}C_6(CO)_{36}]^{6-}$ and $[Ni_{38}C_6(CO)_{42}]^{6-}$. Fig. 13 shows the truncated octahedral geometry of the 410-CVE hexa-anion $[Ni_{32}C_6(CO)_{36}]^{6-}$ and its voltammetric behavior in MeCN solution [14].

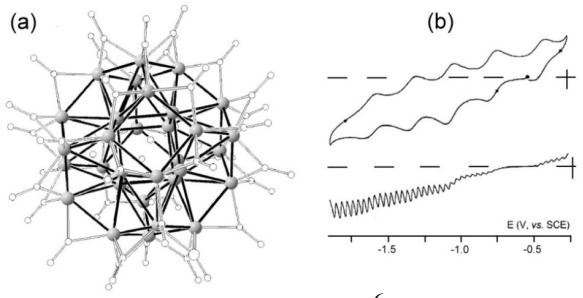

Figure 13. (a) Crystal structure of $[Ni_{32}C_6(CO)_{36}]^{6-}$. (b) Cyclic (top) and hydrodynamic (bottom) voltammograms recorded at a platinum electrode in MeCN solution. Scan rate 0.2 Vs^{-1}.

As seen, joint cyclic and hydrodynamic voltammetric techniques allow detecting that the Ni_{32} cluster undergoes four sequential reductions and one oxidation possessing features of chemical reversibility in the short timescale of cyclic voltammetry. Nevertheless, under the longer times of macroelectrolysis, only $[Ni_{32}C_6(CO)_{36}]^{7-}$ appears perfectly stable.

The formal electrode potentials of the mentioned redox processes are summarized in Table 4, together with those of the related $[Ni_{38}C_6(CO)_{42}]^{6-}$ below discussed.

Table 4. Formal electrode potentials [V, *vs*. SCE] for the electron transfer processes exhibited by the nickel clusters under discussion. MeCN solution.

Complex	Redox processes				
	$E^{\circ\prime}_{5-/6-}$	$E^{\circ\prime}_{6-/7-}$	$E^{\circ\prime}_{7-/8-}$	$E^{\circ\prime}_{8-/9-}$	$E^{\circ\prime}_{9-/10-}$
$[Ni_{32}C_6(CO)_{36}]^{6-}$	–0.45	–0.77	–1.06	–1.33	–1.61
$[Ni_{38}C_6(CO)_{42}]^{6-}$	–0.49	–0.98	–1.33	–1.73	-

The crystal structure of the 482-CVE homologue hexa-anion $[Ni_{38}C_6(CO)_{42}]^{6-}$ is available in the protonated form $[HNi_{38}C_6(CO)_{42}]^{5-}$ [15]. It substantially possesses the same truncated octahedral geometry than $[Ni_{32}C_6(CO)_{36}]^{6-}$ with the additional presence of six Ni(CO) units in the outer surface. Its electrochemical behavior is shown in Fig. 14 [14].

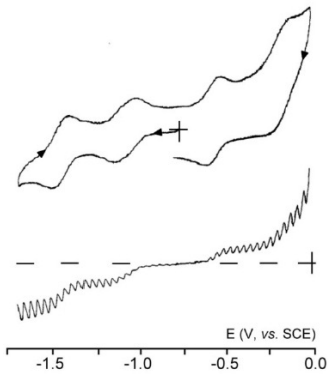

Figure 14. Cyclic (top) and hydrodynamic (bottom) voltammograms recorded at a platinum electrode in MeCN solution of $[Ni_{38}C_6(CO)_{42}]^{6-}$. Scan rate 0.2 Vs^{-1}.

In this case, because of the cathodic shift of all the processes with respect to $[Ni_{32}C_6(CO)_{36}]^{6-}$, the accessibility to different redox steps is more limited.

Heterometallic clusters

Most uncommon chemical and physicochemical properties of heteronuclear derivatives, including metal-carbonyl clusters, arise from synergistic effects of their polar metal–metal bonds [3a].

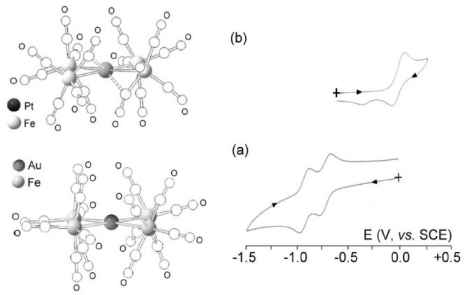

Figure 15. Molecular structures and cyclic voltammetric responses (recorded at platinum working electrode in MeCN solutions) of: (a) $[Fe_4Au(CO)_{16}]^-$ (scan rate 0.2 Vs^{-1}); (b) $[Fe_4Pt(CO)_{16}]^{2-}$ (scan rate 2.0 Vs^{-1}).

$[Fe_4Au(CO)_{16}]^-$ vs. $[Fe_4Pt(CO)_{16}]^{2-}$

The comparison of the electrochemical behavior of the isoelectronic (76-CVE) and substantially isostructural $[Fe_4Au(CO)_{16}]^-$ [16, 17] and $[Fe_4Pt(CO)_{16}]^{2-}$ [17, 18] illustrated in Fig. 15, is exemplificative of the unforeseen role played by the "bimetallic effect" on the redox activity of metal carbonyl clusters.

As seen, the Fe_4Au monoanion undergoes reversibly the sequence –/2– (E°' = –0.73 V, *vs*. SCE) and 2–/3– (E°' = –0.93 V), whereas the Fe_4Pt dianion only undergoes the partially chemically reversible oxidation 2–/– (E°' = +0.01 V).

$[Fe_3Pt_3(CO)_{15}]^{2-}$

The raft-like geometry of the 86-CVE dianion $[Fe_3Pt_3(CO)_{15}]^{2-}$ is illustrated in Fig. 16 [17,19] together with its cyclic voltammetric response [20].

It reversibly undergoes the sequential oxidation processes $[Fe_3Pt_3(CO)_{15}]^{2-/1-/0}$ at potential values: E°' = +0.19 V and −0.40 V, respectively; V *vs*. SCE. In confirmation, the crystal structures of both the monoanion and the neutral congeners are available, [19, 21] and a few pertinent bond lengths are reported in Table 5.

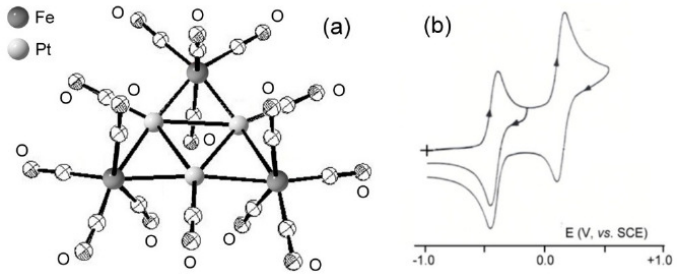

Figure 16. (a) Crystal structure of $[Fe_3Pt_3(CO)_{15}]^{2-}$. (b) Cyclic voltammogram recorded at a platinum electrode in CH_2Cl_2 solution. Scan rate 0.2 Vs^{-1}.

Table 5. Selected averaged bond lengths (Å) of the clusters $[Fe_3Pt_3(CO)_{15}]^{2-/1-/0}$.

Complex	Pt-Pt	Pt-Fe
$[Fe_3Pt_3(CO)_{15}]^{2-}$	2.75	2.60
$[Fe_3Pt_3(CO)_{15}]^{-}$	2.66	2.59
$[Fe_3Pt_3(CO)_{15}]^{0}$	2.59	2.58

The significant shortening of the Pt-Pt distances and the substantially unchanged Pt-Fe distances indicate that the HOMO of the dianion is antibonding with respect to the three platinum atoms.

$[Co_{10}RhN_2(CO)_{21}]^{3-}$ vs. $[Co_{11}N_2(CO)_{21}]^{3-}$

An example concerned with the unforeseen role of the synergistic effects of heterometallic vs. homometallic derivatives is offered by the 154-CVE species $[Co_{10}RhN_2(CO)_{21}]^{3-}$ and the already examined $[Co_{11}N_2(CO)_{21}]^{3-}$.

Fig. 17 gives an overall picture of the structure and electrochemistry of the two derivatives.

The metal frame of $[Co_{10}RhN_2(CO)_{21}]^{3-}$ can be seen as composed of two capped trigonal prisms (each containing an interstitial nitrido atom) that share a triangular face [22], whereas, as already discussed in section 2.1, $[Co_{11}N_2(CO)_{21}]^{3-}$ is composed by two octahedrons having a common vertex (each containing an interstitial nitrido atom) [5b].

The comparison with $[Co_{11}N_2(CO)_{21}]^{3-}$ (which undergoes three one-electron reductions and a two-electron oxidation; see Table 1), shows that $[Co_{10}RhN_2(CO)_{21}]^{3-}$ has a more limited electron transfer aptitude. In fact, it displays either a single one-electron reduction (E°' = −1.06 V) or an apparent two-electron oxidation (E°' = −0.24 V), both complicated by chemical reactions [22].

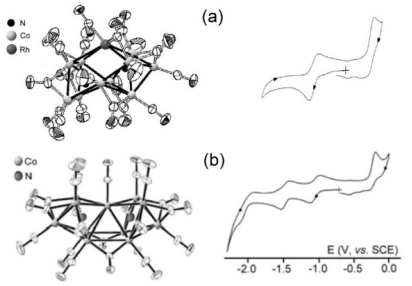

Figure 17. (a) Crystal structure and cyclic voltammogram of $[Co_{10}RhN_2(CO)_{21}]^{3-}$ (CH_3CN solution); platinum electrode; scan rate 0.2 Vs^{-1}. (b) Crystal structure and cyclic voltammogram of $[Co_{11}N_2(CO)_{21}]^{3-}$ (CH_3CN solution); platinum electrode; scan rate 0.2 Vs^{-1}.

$[M_6M'_6(CO)_{24}(L)]^{n-}$

With the general formula $[M_6M'_6(CO)_{24}(L)]^{n-}$, we intend to include $[Fe_6Pd_6(CO)_{24}(H)]^{3-}$, $[Fe_6Ni_6(CO)_{24}(N_2)]^{2-}$ and $[Ru_6Pd_6(CO)_{24}]^{2-}$.

As schematized in Fig. 18, the isostructural $[Fe_6Pd_6H(CO)_{24}]^{3-}$ (160-CVE) [18] and $[Ru_6Pd_6(CO)_{24}]^{2-}$ (158-CVE) [23], are constituted by a trigonally distorted octahedron of Pd atoms capped by six Fe/Ru atoms.

$[Pd_6Ru_6(CO)_{24}]^{2-}$ displays two chemically reversible one-electron oxidations, whereas $[Fe_6Pd_6H(CO)_{24}]^{3-}$ exhibits only a single oxidation. In both cases, the chemical stability of the one-electron oxidation has been proved by controlled potential coulometry. As far as the cathodic behavior is concerned, $[Fe_6Pd_6H(CO)_{24}]^{3-}$ exhibits two one-electron reductions, that are coupled to slow chemical complications. In turn, $[Pd_6Ru_6(CO)_{24}]^{2-}$ apparently also gives rise to two reduction processes coupled to chemical complications, but, in reality, as deducible from the voltammogram at high scan rates shown in the inset, it gives rise to a reversible two-electron reduction affording the short lived congener $[Pd_6Ru_6(CO)_{24}]^{4-}$.

The formal electrode potentials of the mentioned redox changes are compiled in Table 6, together with those of the below discussed dianion $[Fe_6Ni_6(CO)_{24}(N_2)]^{2-}$.

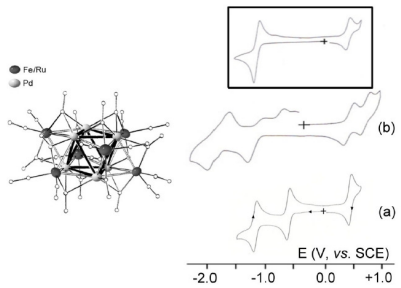

Figure 18. Cyclic voltammograms recorded at platinum electrode in Me_2CO solutions of: (a) $[Fe_6Pd_6H(CO)_{24}]^{3-}$; (b) $[Pd_6Ru_6(CO)_{24}]^{2-}$. Scan rates: (a, b) 0.05 Vs^{-1}; (inset) 20.4 Vs^{-1}.

Finally, Fig. 19a shows the crystal structure of the 168-CVE dianion $[Fe_6Ni_6N_2(CO)_{24}]^2$ (in which the metal frame forms three octahedral cavities, the

two external being filled by the two interstitial nitrides), together with its cyclic voltammetric response in MeCN solution, Fig. 19b [24].

Table 6. Formal electrode potentials [V, *vs*. SCE] for the electron transfer processes exhibited by the clusters $[M_6M'_6(CO)_{24}(L)]^{n-}$.

Complex	Reduction processes			Oxidation processes			Solvent
	$E°'_{2-/3-}$	$E°'_{3-/4-}$	$E°'_{4-/5-}$	$E°'_{3-/2-}$	$E°'_{2-/-}$	$E°'_{-/0}$	
$[Fe_6Pd_6H(CO)_{24}]^{3-}$	-	−0.64	−1.18	+0.39	-	-	Me_2CO
$[Ru_6Pd_6(CO)_{24}]^{2-}$	-	−1.09	−1.09	-	+0.41	+0.65	Me_2CO
$[Fe_6Ni_6(CO)_{24}(N_2)]^{2-}$	−0.40	−0.90	-	-	+0.17	-	MeCN

The dianion exhibits a (coulometrically measured) one-electron oxidation, which possesses features of partial chemical reversibility, as well as two stepwise (coulometrically measured) one-electron reductions, which are chemically reversible both in the cyclic voltammetric and in the macroelectrolysis timescales, Table 6.
In agreement with the chemical reversibility of the reduction processes, the crystal structures of the members of the whole sequence $[Fe_6Ni_6N_2(CO)_{24}]^{2-/3-/4-}$ have been solved. As expected on the basis of the electrochemical reversibility, the variations in metal-metal bonds are rather limited, Table 7.

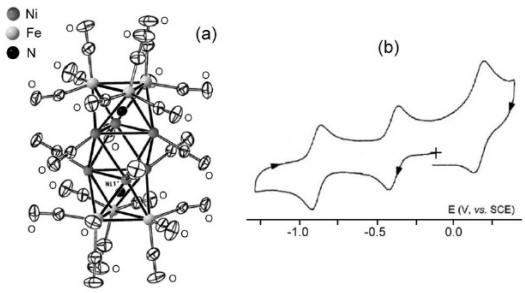

Figure 19. (a) Molecular structure of $[Fe_6Ni_6N_2(CO)_{24}]^{2-}$. (b) Cyclic voltammogram recorded at a platinum electrode in CH_3CN solution. Scan rate 0.5 Vs^{-1}.

Table 7. Selected averaged bond lengths (Å) of the clusters $[Fe_6Ni_6N_2(CO)_{24}]^{n-}$.

Complex	Fe-Ni	Fe-Fe	Ni-Ni$_{(intra\text{triangle})}$	Ni-Ni$_{(inter\text{triangle})}$
$[Fe_6Ni_6N_2(CO)_{24}]^{2-}$	2.63	2.61	2.79	2.62
$[Fe_6Ni_6N_2(CO)_{24}]^{3-}$	2.63	2.62	2.80	2.65
$[Fe_6Ni_6N_2(CO)_{24}]^{4-}$	2.63	2.62	2.81	2.72

The fact that only the Ni–Ni bonds monotonically increase with the increase of the number of valence electrons, suggests that the electron additions enter the central octahedron and populate an antibonding orbital.

$[Co_8Pt_4C_2(CO)_{24}]^{2-}$

The crystal structure of the 170-CVE dicarbide dianion $[Co_8Pt_4C_2(CO)_{24}]^{2-}$ and its cyclic voltammetric pattern are presented in Fig. 20 [25].

The molecular structure closely resembles those previously reported for $[Co_{11}RhN_2(CO)_{24}]^{2-}$ and $[Fe_6Ni_6N_2(CO)_{24}]^{n-}$ (n = 2-4), in that, its metal cage consists on a face-sharing trioctahedron in which the two external assemblies encapsulate a carbide atom.
From the electrochemical viewpoint, $[Co_8Pt_4C_2(CO)_{24}]^{2-}$ undergoes two reduction processes possessing features of chemical reversibility (E°' = –0.91 V and E°' = –1.38 V, *vs*. SCE) and two oxidation processes, only the first one being chemically reversible (E° = +0.18 V), whereas the most anodic process is coupled to chemical complications (E°' = +0.77 V).

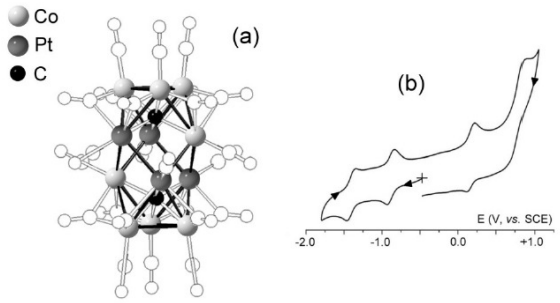

Figure 20. (a) Crystal structure of $[Co_8Pt_4C_2(CO)_{24}]^{2-}$. (b) Cyclic voltammogram recorded at a gold electrode in THF solution. Scan rate 0.2 Vs^{-1}.

As a matter of fact the monoanion $[Co_8Pt_4C_2(CO)_{24}]^{-}$ has been crystallographically characterized [25] and a few significant structural parameters are reported in Table 8.

Table 8. Selected averaged bond lengths (Å) of the clusters $[Co_8Pt_4C_2(CO)_{24}]^{n-}$.

Complex	Co-Co$_{(outer\ \text{triangle})}$	Co-Pt$_{(inner\ \text{triangle})}$	Co-Pt$_{(outer\ centred\ \text{octahedron})}$	Co-Pt$_{(inner\ noncentred\ \text{octahedron})}$
$[Co_8Pt_4C_2(CO)_{24}]^{2-}$	2.62	3.20	2.70	2.69
$[Co_8Pt_4C_2(CO)_{24}]^{-}$	2.62	3.22	2.68	2.75

As seen, as in the case of $[Fe_6Ni_6N_2(CO)_{24}]^{n-}$, the fragment involved in the electron transfer process is the inner octahedron.

$[Ag_{13}Fe_8(CO)_{32}]^{3-}$

The molecular structure of the 226-CVE trianion $[Ag_{13}Fe_8(CO)_{32}]^{3-}$, which is illustrated in Fig. 21, consists of a centered cuboctahedron of silver atoms with the triangular faces capped by $Fe(CO)_4$ units [26].
The pertinent cyclic voltammogram, Fig. 21b, shows that the trianion in MeCN solution undergoes reversibly the reduction to the corresponding $[Ag_{13}Fe_8(CO)_{32}]^{4-}$ (E°' = –0.37 V, *vs*. SCE) and $[Ag_{13}Fe_8(CO)_{32}]^{5-}$ (E°' = –0.65 V). As a consequence, such tetra- and penta-anions have been structurally characterized [27,28] and a few bond lengths for the sequence $[Ag_{13}Fe_8(CO)_{32}]^{3-/4-/5-}$ are summarized in Table 9.

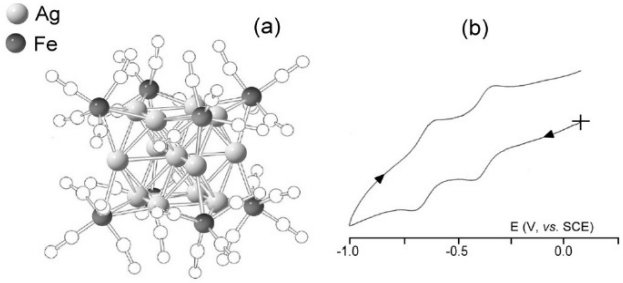

Figure 21. (a) Crystal structure of $[Ag_{13}Fe_8(CO)_{32}]^{3-}$. (b) Cyclic voltammogram recorded at a gold electrode in MeCN solution. Scan rate 0.2 Vs^{-1}.

Table 9. Selected averaged bond lengths (Å) of the clusters $[Ag_{13}Fe_8(CO)_{32}]^{n-}$.

Complex	Ag-Ag	Ag-Fe
$[Ag_{13}Fe_8(CO)_{32}]^{3-}$	2.93	2.71
$[Ag_{13}Fe_8(CO)_{32}]^{4-}$	2.92	2.74
$[Ag_{13}Fe_8(CO)_{32}]^{5-}$	2.90	2.75

Since the distances Ag-Ag tend to decrease and the Ag-Fe tend to increase with the addition of electrons, it is evident that the LUMOs of the cluster are bonding with respect to the Ag-cuboctahedron and antibonding with respect to the Fe-capping subunits.

$[Os_{18}Pd_3(C)_2(CO)_{42}]^{2-}$

The 268-CVE dicarbide dianion $[Os_{18}Pd_3(C)_2(CO)_{42}]^{2-}$ possesses the quite spectacular structure shown in Fig. 22a, which can be described as a triangular Pd_3 metal unit sandwiched between two tricapped octahedral $\{Os_9(\mu_6\text{-}C)(CO)_{21}\}$ subclusters [29].

As illustrated in Fig. 22b, the dianion undergoes five reversible reductions at E°' = +0.17 V, −0.21 V, −0.77 V, −1.20 V, −1.71 V (V, *vs*. SCE). The asterisked reduction process at −1.63 V is attributed to the $[N(PPh_3)_2]^+$ counterion.

We note that the present cluster is isostructural with the 274-CVE dianion $[Os_{18}Hg_3(C)_2(CO)_{42}]^{2-}$ [30], which however possesses a markedly lower redox activity [31].

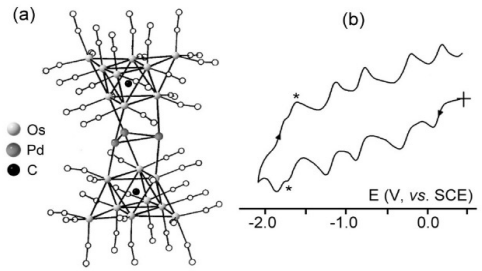

Figure 22. (a) Crystal structure of $[Os_{18}Pd_3(C)_2(CO)_{42}]^{2-}$. (b) Cyclic voltammogram recorded at a glassy carbon electrode in Me_2CO solution. Scan rate 0.2 Vs^{-1}.

$[Ni_{38}Pt_6(CO)_{48}]^{6-}$

As illustrated in Fig. 23a, the metal frame of the 542-CVE hexaanion $[Ni_{38}Pt_6(CO)_{48}]^{6-}$ can be represented by an octahedron of platinum atoms encapsulated in a (ν_3) macro-tetrahedron constituted by 38 nickel atoms. Such a geometrical organization is structurally proved by crystal structure of the protonated congener $[Ni_{38}Pt_6(CO)_{48}H]^{5-}$ [32].

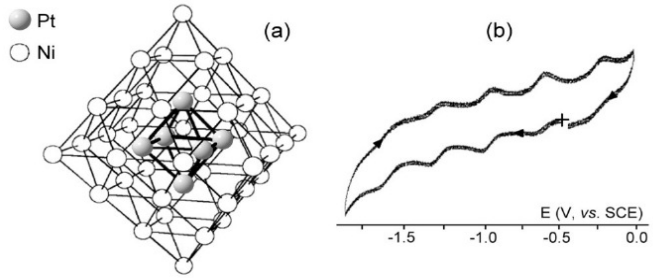

Figure 23. (a) Crystal structure of $[Ni_{38}Pt_6(CO)_{48}H]^{5-}$. (b) Cyclic voltammogram recorded at a platinum electrode in DMF solution of $[Ni_{38}Pt_6(CO)_{48}]^{6-}$. Scan rate 0.2 Vs^{-1}.

As shown in Fig. 23b, the hexaanion displays a rich redox aptitude exhibiting five one-electron redox processes [namely, one oxidation ($E^{\circ\prime}$ = –0.62 V, *vs.* SCE) and four reductions ($E^{\circ\prime}$ = –0.97 V, –1.29 V, –1.54 V and –1.75 V, respectively)] having features of chemical and electrochemical reversibility in the cyclic voltammetric time scale.

Conclusion

We have focused on the electrochemical behavior of a series of high-nuclearity metal-carbonyl clusters able to give rise to sequences of reversible, one-electron transfer processes in order to attest their potential use in molecular electronics. In particular, we tried to support their possible use as nanocapacitors proving that they afford consecutive redox processes separated by finite differences in potential values. Such a parameter, preluding to their semiconducting nature, is crucial to the accurate control of the flow of electrons needed to charge the device. The event has not to be neglected in that in conducting materials the capacitor charging proceeds through an uncontrolled cascade of electrons. In fact, we gave evidence that the transition from semiconductor to metallic conductor takes place for metal-carbonyl clusters having nuclearities above a likely threshold value of *ca*. 70 [33].

Acknowledgements

Piero Zanello gratefully acknowledges the financial support of the Italian MIUR (PRIN 2008).

References

1. (a) C. Femoni, M.C. Iapalucci, F. Kaswalder, G. Longoni, S. Zacchini, *Coord. Chem. Rev.* 250 (2006) 1580.
   (b) U. Simon, On the possibility of single electronics based on ligand-stabilized metal clusters, *in* Metal clusters in chemistry. Vol. 3, P. Braunstein, L.A. Oro, P.R. Raithby (eds), Wiley–VCH Weinheim, (1999) pp 1342–1359.
   (c) G. Schmid, Y.P. Liu, M. Schumann, T. Raschke, C. Radehaus, *Nano Lett.* 1 (2001) 405.
   (d) S. Hoeppener, L. Chi, H. Fuchs, *Nano Lett.* 2 (2002) 459.
   (e) M.H.V. Werts, M. Lambert, J-P. Bourgoin, M. Brust, *Nano Lett*. 2 (2002) 43.
   (f) A.C. Templeton, W.P. Wuelfing, R.W. Murray, *Acc. Chem. Res.* 33 (2000) 27.
   (g) L.F. Chi, M. Hartig, T. Drechsler, T. Schwaack, C. Seidel, H. Fuchs, G. Schmid, *Appl. Phys. Lett.* 66 (1998) S187.
   (h) R.L. Carroll, C.D. Gorman, *Angew. Chem. Int. Ed.* 41 (2002) 4378.
   (i) J. Sinzig, L.J.de Jongh, A. Cerotti, R. Della Pergola, G. Longoni, M. Stener, K. Albert, N. Rosch, *Phys. Rev. Lett.* 81 (1998) 3211.
2. (a) D. Collini, C. Femoni, M.C. Iapalucci, G. Longoni, P.H. Svensson, P. Zanello, *Angew. Chem. Int. Ed.* 41 (2002) 3685-3688.
   (b) V. G. Albano, F. Demartin, M.C. Iapalucci, F. Laschi, G. Longoni, A. Sironi, P. Zanello, *J. Chem. Soc., Dalton Trans.* (1991) 739.
3. (a) P. Zanello, Stereochemical aspects associated with the redox behavior of heterometal carbonyl clusters, *Struct. Bonding (Berlin)* 79 (1992) 101.
   (b) P. Zanello, The redox propensity of high nuclearity metal clusters "NATO ASI Series", Series C: Mathematical and Physical Sciences, Kluwer Academic Publishers, Vol. 385, 1993, p. 229.
   (c) P. Zanello, Stereochemical aspects of the redox propensity of homometal carbonyl clusters, in "Stereochemistry of Organometallic and Inorganic Compounds", P.Zanello, ed. Elsevier, Amsterdam; Vol. 5, (1994) 163-408.
   (d) P. Zanello, F. Fabrizi de Biani, Bimetallic effects on the redox activity of transition-metal carbonyl clusters, in Metal Clusters in Chemistry, P. Braunstein, L.A. Oro, P.R. Raithby, Eds., Wiley-VCH, Vol. 2, 1999, 1104-1136.
   (e) G. Longoni, C. Femoni, M.C. Iapalucci and P. Zanello, Electron-sink features of homoleptic transition-metal carbonyl clusters, in Metal Clusters in Chemistry, P. Braunstein, L.A. Oro, P.R. Raithby Eds., Wiley-VCH, Vol. 2, 1999, 1137-1158.
   (f) P. Zanello, Structure and electrochemistry of transition metal carbonyl clusters with interstitial or semi-interstitial atoms: contrast between nitrides or phosphides and carbides, in Physical Organometallic Chemistry. Vol. 3: Unusual Structures and Physical Properties in Organometallic Chemistry. M. Gielen, R. Willem, B. Wrackmeyer, eds., John Wiley, Chichester, UK., 2002, pp. 1-49.

4. G. Ciani, A. Sironi, S. Martinego, L. Garlaschelli, R. Della Pergola, P. Zanello, F. Laschi, N. Masciocchi, *Inorg. Chem.* 40 (2001) 3905.
5. (a) A. Fumagalli, S. Martinengo, M. Tasselli, G. Ciani, P. Macchi, A. Sironi, *Inorg. Chem.* 37 (1998) 2826.
(b) A. Fumagalli, P. Ulivieri, M. Costa, O. Crispu, R. Della Pergola, F. Fabrizi De Biani, F. Laschi, P. Zanello, P. Macchi, A. Sironi, *Inorg. Chem.* 43 (2004) 2125.
6. (a) V.G. Albano, D. Braga, P. Chini, G. Ciani and S. Martinengo, *J. Chem. Soc., Dalton Trans.* (1982) 645.
(b) A. Fumagalli, M. Costa, R. Della Pergola, P. Zanello, F. Fabrizi de Biani, P. Macchi, A. Sironi, *Inorg. Chim. Acta* 350 (2003) 1006.
7. R. Della Pergola, F. Demartin, L. Garlaschelli, M. Manassero, S. Martinengo, N. Masciocchi and P. Zanello, *Inorg. Chem.* 32 (1993) 3670.
8. R. Della Pergola, L. Garlaschelli, M. Manassero, N. Masciocchi, P. Zanello, *Angew. Chem., Int. Ed. Engl.* 32 (1993) 1347.
9. D.M. Washecheck, E.J. Wucherer, L.F. Dahl, A. Ceriotti, G. Longoni, M. Manassero, M. Sansoni, P. Chini, *J. Am. Chem. Soc.* 101 (1979) 6110.
10. S. Fedi, P. Zanello, F. Laschi, A. Ceriotti, S. El Afefey, *J. Solid State Electrochem.* 13 (2009) 1497.
11. (a) G.J. Lewis, J.D. Roth, R.A. Montag, L.K. Safford, X. Gao, S.-C. Chang, L.F. Dahl, M.J. Weaver, *J. Am. Chem. Soc.* 112 (1990) 2831.
(b) J.D. Roth, G.J. Lewis, L.K. Safford, X. Jiang, L.F. Dahl, M.J. Weaver, *J. Am. Chem. Soc.* 114 (1992) 6159.
12. A. Ceriotti, N. Masciocchi, P. Macchi, G. Longoni, *Angew. Chem. Int. Ed.* 38 (1999) 3724.
13. A.J. Amoroso, L.H. Gade, B.F.G. Johnson, J. Lewis, P.R. Raithby, W.-T. Wong, *Angew. Chem, Int. Ed. Engl.* 30 (1991) 107.
14. F. Calderoni, F. Demartin, F. Fabrizi de Biani, C. Femoni, M.C. Iapalucci, G. Longoni, P. Zanello, *Eur. J. Inorg. Chem.* (1999) 663.
15. A. Ceriotti, A. Fait, G. Longoni, G. Piro, F. Demartin, M. Manassero, N. Masciocchi, M. Sansoni, *J. Am. Chem. Soc.* 108 (1986) 8091.
16. V.G. Albano, R. Aureli, M.C. Iapalucci, F. Laschi, G. Longoni, M. Monari, P. Zanello, *J. Chem. Soc., Chem. Commun.* (1993) 1501.
17. C. Femoni, M.C. Iapalucci, G. Longoni, C. Tiozzo, J. Wolowska, S. Zacchini, E. Zazzaroni, *Chem. Eur. J.* 13 (2007) 6544.
18. G. Longoni, M. Manassero, M. Sansoni, *J. Am. Chem. Soc.* 102 (1980) 3242.
19. G. Longoni, M. Manassero, M. Sansoni, *J. Am. Chem. Soc.* 102 (1980) 7973.
20. R. Della Pergola, L. Garlaschelli, C. Mealli, D.M. Proserpio, P. Zanello, *J. Cluster Sci.* 1 (1990) 93.
21. R.D. Adams, I. Arafa, G. Chen, J.-C. Lii, J.-G. Wang, *Organometallics* 9 (1990) 2350.
22. M. Costa, R. Della Pergola, A. Fumagalli, F. Laschi, S. Losi, P. Macchi, A. Sironi, P. Zanello, *Inorg. Chem.* 46 (2007) 552.

23. E. Brivio, A. Ceriotti, R. Della Pergola, L. Garlaschelli, F. Demartin, M. Manassero, M. Sansoni, P. Zanello, F. Laschi, B.T. Heaton, *J. Chem. Soc., Dalton Trans.* (1994) 3237.
24. R. Della Pergola, M. Bruschi, F. Fabrizi de Biani, A. Fumagalli, L. Garlaschelli, F. Laschi, M. Manassero, M. Sansoni, P. Zanello, *C.R. Chimie* 8 (2005) 1850.
25. C. Femoni, M.C. Iapalucci, G. Longoni, J. Wolowska, S. Zacchini, P. Zanello, S. Fedi, M. Riccò, D. Pontiroli, M. Mazzani, *J. Am. Chem. Soc.* 132 (2010) 2919.
26. V.G. Albano, F. Calderoni, M.C. Iapalucci, G. Longoni, M. Monari, P. Zanello, *J. Cluster Sci.* 6 (1995) 107.
27. V.G. Albano, L. Grossi, G. Longoni, M. Monari, S. Mulley, A. Sironi, *J. Am. Chem. Soc.* 114 (1992) 5708.
28. D. Collini, C. Femoni, M.C. Iapalucci, G. Longoni, *C.R.* Chimie 8 (2005) 1645.
29. K.-F. Yung, W.-T. Wong, *Angew. Chem.* 115 (2003) 571.
30. L.H. Gade, B.F.G. Johnson, J. Lewis, M. MacPartlin, H.R. Powell, *J. Chem. Soc., Chem. Commun.* (1990) 110.
31. *L.H. Gade, B.F.G. Johnson, J. Lewis, G. Conole, M. MacPartlin, J. Chem. Soc., Dalton Trans.,* (1992) 3249.
32. A. Ceriotti, F. Demartin, G. Longoni, M. Manassero, M. Marchionna, G. Piva, M. Sansoni, *Angew. Chem., Int. Ed. Engl.* 24 (1985) 696.
33. F. Fabrizi de Biani, C. Femoni, M.C. Iapalucci, G. Longoni, P. Zanello, A. Ceriotti, *Inorg. Chem.* 38 (1999) 3721.